

# Prospects on Compositeness and New Vector Bosons at LC with Polarization<sup>1</sup>

A.A. Pankov

Technical University of Gomel, 246746 Gomel  
Belarus

## Abstract

Fermion compositeness, and other new physics which can be described by an exchange of very massive particles ( $Z'$  boson, leptoquarks, sparticles with  $R$ -parity violating couplings), can be manifest itself as the presence of a strong four-fermion contact interaction. For the processes  $e^+e^- \rightarrow \mu^+\mu^-$ ,  $\tau^+\tau^-$ ,  $\bar{b}b$  and  $\bar{c}c$  at a future  $e^+e^-$  linear collider (LC) with  $\sqrt{s} = 0.5$  TeV, we examine the sensitivity of the helicity cross sections to four-fermion contact interactions. If longitudinal polarization of the electron beam were available, two polarized integrated cross sections would offer the opportunity to separate the helicity cross sections and, in this way, to derive model-independent bounds on the relevant parameters. The measurement of these polarized cross sections with optimal kinematical cuts could significantly increase the sensitivity of helicity cross sections to contact interaction parameters and could give crucial information on the chiral structure of such new interactions. In addition, we consider the application of the proposed approach to the search for manifestations of a  $Z'$  for typical extended model examples.

## 1 Introduction and separation of the helicity cross sections

Deviations from the Standard Model (SM) caused by new physics characterized by very high mass scales  $\Lambda$  can systematically be studied at lower energies by using the effective Lagrangian approach. The effects of the new physics can be observed at energies well-below  $\Lambda$ , and can be related to some effective contact interaction [1, 2]. In the framework of composite models of leptons and quarks, the contact interaction is regarded as a remnant of the binding force between the fermion substructure constituents. Furthermore, in  $e^+e^-$  collisions, many types of new physics, for which the exchanged particles in the  $s$ ,  $t$ , or  $u$  channels have mass-squared much larger than the corresponding Mandelstam invariant variables, can be described by an effective  $eff$  contact term in the interaction Lagrangian [3]-[6]. For example, effects of a  $Z'$  boson of a few TeV mass scale would be well-represented by a four-fermion contact interaction. The exchange of a leptoquark of a similar mass scale could be described by an effective  $eqq$  contact term in the relevant interaction. At energies much lower than the sparticle masses,  $R$ -parity breaking interactions introduce effective  $ell$  and  $eqq$  interactions. Thus, quite generally, the contact interaction is considered as a convenient parameterization of deviations from the SM that may be caused by some new physics at the large scale  $\Lambda$ .

Fermion-pair production in  $e^+e^-$  collisions

$$e^+ + e^- \rightarrow \bar{f} + f \quad (1)$$

( $f = l$  or  $q$ ) is one of the basic processes of the SM, and deviations of the measured observables from the predicted values would be a first indication of new physics beyond the SM.

The lowest-order four-fermion contact terms have dimension  $D = 6$ , which implies that they are suppressed by  $g_{\text{eff}}^2/\Lambda^2$ . Restricting the fermion currents to be helicity conserving and flavor diagonal, the general  $SU(3) \times SU(2) \times U(1)$  invariant four-fermion  $eff$  contact interaction Lagrangian with  $D = 6$  can be written as [1]-[7]:

$$\mathcal{L} = \frac{g_{\text{eff}}^2}{\Lambda^2} [\eta_{LL} (\bar{e}_L \gamma_\mu e_L) (\bar{f}_L \gamma^\mu f_L) + \eta_{LR} (\bar{e}_L \gamma_\mu e_L) (\bar{f}_R \gamma^\mu f_R) + \eta_{RL} (\bar{e}_R \gamma_\mu e_R) (\bar{f}_L \gamma^\mu f_L) + \eta_{RR} (\bar{e}_R \gamma_\mu e_R) (\bar{f}_R \gamma^\mu f_R)], \quad (2)$$

where generation and color indices have been suppressed. It is conventional to take  $g_{\text{eff}}^2 = 4\pi$  and  $\eta_{\alpha\beta} = \pm 1$  ( $\alpha, \beta = L, R$ ).

<sup>1</sup>Talk given at the International Workshop QFTHEP'99, Moscow, May 27 - June 2, 1999

In general, for a given fermion flavor  $f$ , Eq. (2) defines eight independent, individual interaction models corresponding to the combinations of the four chiralities LL, LR, RL and RR with the  $\pm$  signs of the  $\eta$ 's. In practice, the true interaction might correspond to one of these models or to any combination of them. Here, we will perform a model-independent analysis of the contact interactions.

In principle, the sought-for deviations of observables from the SM predictions, giving information on  $\Lambda$ 's, simultaneously depend on all four-fermion effective coupling constants in Eq. (2), which therefore cannot be easily disentangled. For simplicity, the analysis is usually performed by taking a non-zero value for only one parameter at a time, all the remaining ones being put equal to zero. Limits on individual  $eeqq$  contact interaction parameters have recently been derived by this procedure, from a global analysis of the relevant data [7], and the individual models are severely constrained, with  $\Lambda_{\alpha\beta} \sim \mathcal{O}(10)$  TeV. However, if several terms of different chiralities were simultaneously taken into account, cancellations may occur and the resulting bounds on  $\Lambda_{\alpha\beta}$  would be considerably weaker, of the order of 3 – 4 TeV. Consequently, a definite improvement of the situation in this regard should be obtained from a procedure of analyzing experimental data that allows to account for the various contact interaction couplings simultaneously as free parameters, and yet to obtain in a model-independent way separate bounds for the corresponding  $\Lambda$ 's, not affected by possible accidental cancellations. In this paper we shall propose an analysis of  $eell$ ,  $eebb$  and  $eecc$  contact interactions at the next linear  $e^+e^-$  collider with  $\sqrt{s} = 500$  GeV and with longitudinally polarized beams. Our approach makes use of two particular, polarized, integrated cross sections  $\sigma_1$  and  $\sigma_2$ , that are directly connected, *via* linear combinations, to the helicity cross sections of process (1), and therefore allow to deal with a minimal set of independent free parameters.

This kind of observables, defined for specific kinematical cuts, were already introduced to study  $Z'$  signals at LEP2 and LC [8, 9] and potential manifestations of compositeness at the LC [10]. Here, we extend the previous considerations by performing a general analysis where, in the definition of the above-mentioned integrated observables, we choose suitable kinematical regions where the sensitivity to individual four-fermion contact interaction parameters is maximal. Also, an application of the proposed approach to  $Z'$  searches at LC is discussed where, in particular, the constraints on the relevant parameters are derived.

In the Born approximation, including the  $\gamma$  and  $Z$  exchanges as well as the four-fermion contact interaction term (2), but neglecting  $m_f$  with respect to the c.m. energy  $\sqrt{s}$ , the differential cross section for the process  $e^+e^- \rightarrow ff$  ( $f \neq e, t$ ) with longitudinally polarized electron-positron beams, can be written as

$$\frac{d\sigma}{d\cos\theta} = \frac{3}{8} [(1 + \cos\theta)^2 \sigma_+ + (1 - \cos\theta)^2 \sigma_-], \quad (3)$$

where  $\theta$  is the angle between the incoming electron and the outgoing fermion in the c.m. frame. The functions  $\sigma_{\pm}$  can be expressed in terms of helicity cross sections

$$\sigma_{\alpha\beta} = N_C \sigma_{\text{pt}} |A_{\alpha\beta}|^2. \quad (4)$$

Here,  $N_C$  is the QCD factor:  $N_C \approx 3(1 + \alpha_s/\pi)$  for quarks and  $N_C = 1$  for leptons, respectively, and  $\sigma_{\text{pt}} \equiv \sigma(e^+e^- \rightarrow \gamma^* \rightarrow l^+l^-) = (4\pi\alpha^2)/(3s)$ . With electron and positron longitudinal polarizations  $P_e$  and  $P_{\bar{e}}$ , the relations are

$$\sigma_+ = \frac{1}{4} [(1 - P_e)(1 + P_{\bar{e}}) \sigma_{\text{LL}} + (1 + P_e)(1 - P_{\bar{e}}) \sigma_{\text{RR}}], \quad (5)$$

$$\sigma_- = \frac{1}{4} [(1 - P_e)(1 + P_{\bar{e}}) \sigma_{\text{LR}} + (1 + P_e)(1 - P_{\bar{e}}) \sigma_{\text{RL}}]. \quad (6)$$

The helicity amplitudes  $A_{\alpha\beta}$  can be written as

$$A_{\alpha\beta} = Q_e Q_f + g_{\alpha}^e g_{\beta}^f \chi_Z + \frac{s\eta_{\alpha\beta}}{\alpha\Lambda_{\alpha\beta}^2}, \quad (7)$$

where the gauge boson propagator is  $\chi_Z = s/(s - M_Z^2 + iM_Z\Gamma_Z)$ , the SM left- and right-handed fermion couplings of the  $Z$  are  $g_L^f = (I_{3L}^f - Q_f s_W^2)/s_W c_W$  and  $g_R^f = -Q_f s_W^2/s_W c_W$  with  $s_W^2 = 1 - c_W^2 \equiv \sin^2 \theta_W$ , and  $Q_f$  are the fermion electric charges.

The total cross section and the difference of forward and backward cross sections are given as

$$\sigma = \sigma_+ + \sigma_- = \frac{1}{4} [(1 - P_e)(1 + P_{\bar{e}})(\sigma_{LL} + \sigma_{LR}) + (1 + P_e)(1 - P_{\bar{e}})(\sigma_{RR} + \sigma_{RL})], \quad (8)$$

$$\begin{aligned} \sigma_{FB} &\equiv \sigma_F - \sigma_B = \frac{3}{4} (\sigma_+ - \sigma_-) \\ &= \frac{3}{16} [(1 - P_e)(1 + P_{\bar{e}})(\sigma_{LL} - \sigma_{LR}) + (1 + P_e)(1 - P_{\bar{e}})(\sigma_{RR} - \sigma_{RL})], \end{aligned} \quad (9)$$

where

$$\sigma_F = \int_0^1 (\frac{d\sigma}{d\cos\theta}) d\cos\theta, \quad \sigma_B = \int_{-1}^0 (\frac{d\sigma}{d\cos\theta}) d\cos\theta. \quad (10)$$

Taking Eq. (7) into account, these relations show that in general  $\sigma$  and  $\sigma_{FB}$  simultaneously involve all contact-interactions couplings even in the polarized case. Therefore, by themselves, these measurements do not allow a completely model-independent analysis avoiding, in particular, potential cancellations among different couplings.

Our analysis will be based on the consideration of the four helicity cross sections  $\sigma_{\alpha\beta}$  as the basic independent observables to be measured from data on the polarized differential cross section. These cross sections depend each on just one individual four-fermion contact parameter and therefore lead to a model-independent analysis where all  $\eta_{\alpha\beta}$  can be taken simultaneously into account as completely free parameters, with no danger from potential cancellations. As Eqs. (5) and (6) show, helicity cross sections can be disentangled *via* the measurement of  $\sigma_+$  and  $\sigma_-$  with different choices of the initial beam polarizations.

One possibility is to project out  $\sigma_+$  and  $\sigma_-$  from  $d\sigma/d\cos\theta$ , as differences of integrated cross sections. To this aim, we define  $z_{\pm}^* \equiv \cos\theta_{\pm}^*$  such that

$$\left( \int_{z_{\pm}^*}^1 - \int_{-1}^{z_{\pm}^*} \right) (1 \mp \cos\theta)^2 d\cos\theta = 0. \quad (11)$$

One finds the solutions:  $z_{\pm}^* = \mp(2^{2/3} - 1) = \mp0.587$  ( $\theta_+^* = 126^\circ$  and  $\theta_-^* = 54^\circ$ ). These values satisfy  $(z_{\pm}^* \mp 1)^3 = \mp 4$ . In the case of  $|\cos\theta| = c < 1$ , one has  $|z_{\pm}^*| = (1 + 3c^2)^{1/3} - 1$ .

From Eq. (3) one can easily see that at these values of  $z_{\pm}^*$  the difference of two integrated cross sections defined as

$$\sigma_1(z_{\pm}^*) - \sigma_2(z_{\pm}^*) \equiv \left( \int_{z_{\pm}^*}^1 - \int_{-1}^{z_{\pm}^*} \right) \frac{d\sigma}{d\cos\theta} d\cos\theta \quad (12)$$

is directly related to  $\sigma_{\pm}$  as:

$$\sigma_1(z_+^*) - \sigma_2(z_+^*) = \gamma\sigma_+, \quad \sigma_2(z_-^*) - \sigma_1(z_-^*) = \gamma\sigma_-, \quad (13)$$

where  $\gamma = 3(2^{2/3} - 2^{1/3}) = 0.982$ .

The solutions of the system of two equations corresponding to  $P_e = \pm P$ , and assuming unpolarized positrons  $P_{\bar{e}} = 0$ , in Eqs. (5) and (6), can be written as:

$$\sigma_{LL} = \frac{1+P}{P}\sigma_+(-P) - \frac{1-P}{P}\sigma_+(P), \quad (14)$$

$$\sigma_{RR} = \frac{1+P}{P}\sigma_+(P) - \frac{1-P}{P}\sigma_+(-P), \quad (15)$$

$$\sigma_{LR} = \frac{1+P}{P}\sigma_-(-P) - \frac{1-P}{P}\sigma_-(P), \quad (16)$$

$$\sigma_{RL} = \frac{1+P}{P}\sigma_-(P) - \frac{1-P}{P}\sigma_-(-P). \quad (17)$$

From Eqs. (14)–(17) one can easily see that this procedure allows to extract  $\sigma_{LL}$ ,  $\sigma_{RR}$ ,  $\sigma_{LR}$  and  $\sigma_{RL}$  by the four independent measurements of  $\sigma_1(z_{\pm}^*)$  and  $\sigma_2(z_{\pm}^*)$  at  $P_e = \pm P$ .

## 2 Optimization and model independent analysis

This extraction of helicity cross sections can be obtained more generally. Indeed, let us divide the full angular range,  $|\cos\theta| \leq 1$  into two parts,  $(-1, z^*)$  and  $(z^*, 1)$ , with arbitrary  $z^*$ , and define two integrated cross sections as

$$\sigma_1(z^*) \equiv \int_{z^*}^1 \frac{d\sigma}{d\cos\theta} d\cos\theta = \frac{1}{8} \{ [8 - (1 + z^*)^3] \sigma_+ + (1 - z^*)^3 \sigma_- \}, \quad (18)$$

$$\sigma_2(z^*) \equiv \int_{-1}^{z^*} \frac{d\sigma}{d\cos\theta} d\cos\theta = \frac{1}{8} \{ (1 + z^*)^3 \sigma_+ + [8 - (1 - z^*)^3] \sigma_- \}. \quad (19)$$

Solving these two equations, one finds the general relations

$$\sigma_+ = \frac{1}{6(1 - z^{*2})} [(8 - (1 - z^*)^3) \sigma_1(z^*) - (1 - z^*)^3 \sigma_2(z^*)], \quad (20)$$

$$\sigma_- = \frac{1}{6(1 - z^{*2})} [-(1 + z^*)^3 \sigma_1(z^*) + (8 - (1 + z^*)^3) \sigma_2(z^*)], \quad (21)$$

that allow to disentangle the helicity cross sections, using (14)–(17) and the availability of polarized beams.

We take radiative corrections into account by means of the program ZFITTER [11], which has to be used along with ZEFT, adapted to the present discussion. Due to the radiative return to the  $Z$  resonance at  $\sqrt{s} > M_Z$ , the energy spectrum of the radiated photons is peaked around  $k_{\text{peak}} \approx 1 - M_Z^2/s$  [12]. In order to increase the signal originating from contact interactions, events with hard photons should be eliminated by an appropriate cut  $\Delta < k_{\text{peak}}$  on the photon energy. For our numerical analysis, we use  $m_{\text{top}} = 175$  GeV,  $m_H = 100$  GeV and a cut  $\sqrt{s'} \geq 0.9\sqrt{s}$  to avoid the radiative return to the  $Z$  peak for  $\sqrt{s} = 0.5$  TeV.

In the case where no deviation from the SM is observed, one can make an assessment of the sensitivity of the process (1) to the contact interaction parameters, based on the expected experimental accuracy on the observables  $\sigma_{\alpha\beta}$ . Such sensitivity numerically determines the bounds on the contact-interaction scales  $\Lambda_{\alpha\beta}$  that can be derived from the experimental data and, basically, is determined by the comparison of deviations from the SM predictions due to the contact-interaction terms with the attainable experimental uncertainty. Accordingly, we define the ‘significance’ of each helicity cross section by the ratio:

$$\mathcal{S} = \frac{|\Delta\sigma_{\alpha\beta}|}{\delta\sigma_{\alpha\beta}}, \quad (22)$$

where  $\Delta\sigma_{\alpha\beta}$  is the deviation from the SM prediction, dominated for  $\sqrt{s} \ll \Lambda_{\alpha\beta}$  by the interference term:

$$\Delta\sigma_{\alpha\beta} \equiv \sigma_{\alpha\beta} - \sigma_{\alpha\beta}^{\text{SM}} \simeq 2N_C \sigma_{\text{pt}} \left( Q_e Q_f + g_\alpha^e g_\beta^f \chi_Z \right) \frac{s\eta_{\alpha\beta}}{\alpha\Lambda_{\alpha\beta}^2}, \quad (23)$$

and  $\delta\sigma_{\alpha\beta}$  is the expected experimental uncertainty on  $\sigma_{\alpha\beta}$ , combining statistical and systematic uncertainties.

For example, adding uncertainties in quadrature, the uncertainty on  $\sigma_{\text{LL}}$ , indirectly measured *via*  $\sigma_1$  and  $\sigma_2$  (see Eqs. (14) and (20)), is given by

$$\begin{aligned} (\delta\sigma_{\text{LL}})^2 &= a^2(z^*) \left( \frac{1+P}{P} \right)^2 (\delta\sigma_1(z^*, -P))^2 + a^2(z^*) \left( \frac{1-P}{P} \right)^2 (\delta\sigma_1(z^*, P))^2 \\ &\quad + b^2(z^*) \left( \frac{1+P}{P} \right)^2 (\delta\sigma_2(z^*, -P))^2 + b^2(z^*) \left( \frac{1-P}{P} \right)^2 (\delta\sigma_2(z^*, P))^2, \end{aligned} \quad (24)$$

where

$$a(z^*) = \frac{8 - (1 - z^*)^3}{6(1 - z^{*2})}, \quad b(z^*) = -\frac{(1 - z^*)^3}{6(1 - z^{*2})}. \quad (25)$$

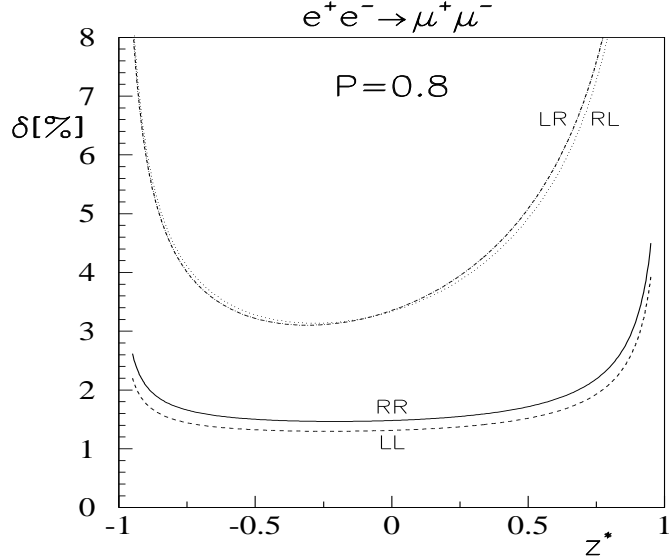


Figure 1: The uncertainty on the helicity cross sections  $\sigma_{\alpha\beta}$  in the SM as a function of  $z^*$  for the process  $e^+e^- \rightarrow \mu^+\mu^-$  at  $\sqrt{s} = 0.5$  TeV,  $\mathcal{L}_{\text{int}} = 50 \text{ fb}^{-1}$ ,  $P = 0.8$ ,  $\epsilon = 95\%$  and  $\delta^{\text{sys}} = 0.5\%$ . Radiative corrections are included.

Analogous expressions hold for the combinations related to the uncertainties  $\delta\sigma_{\text{RR}}$ ,  $\delta\sigma_{\text{LR}}$  and  $\delta\sigma_{\text{RL}}$ . Numerically, in the situation of small deviations from the SM we are considering, we can use to a very good approximation the SM predictions for the cross sections  $\sigma_{1,2}$  to assess the expected  $\delta\sigma_{1,2}$  and therefore of the uncertainties  $\delta\sigma_{\alpha\beta}$  in the denominator of (22). Basically, the directly measured integrated cross sections  $\sigma_{1,2}$  of Eqs. (18) and (19) and, correspondingly, the uncertainties  $\delta\sigma_{\alpha\beta}$ , are dependent on the value of  $z^*$ , which can be considered in general as an input parameter related to given experimental conditions (see, *e.g.*, Eq. (24)). Since the deviation  $\Delta\sigma_{\alpha\beta}$  of Eq. (23) is independent of  $z^*$ , the full sensitivity of a given helicity cross section to the relevant contact-interaction parameter is determined by the corresponding size and  $z^*$  behavior of the uncertainty  $\delta\sigma_{\alpha\beta}$ . Then, the optimization would be obtained by choosing for  $z^*$  the value  $z_{\text{opt}}^*$  where the uncertainty  $\delta\sigma_{\alpha\beta}$  becomes minimum, *i.e.*, where the corresponding sensitivity Eq. (22) has a maximum. As anticipated, we estimate the required  $z^*$  behavior from the known SM cross sections.

Combining, again in quadrature, statistical and systematic uncertainties on  $\sigma_{1,2}$ , we have:

$$(\delta\sigma_i)^2 \simeq (\delta\sigma_i^{\text{SM}})^2 = \frac{\sigma_i^{\text{SM}}}{\epsilon \mathcal{L}_{\text{int}}} + (\delta^{\text{sys}} \sigma_i^{\text{SM}})^2. \quad (26)$$

Numerically, for  $\sigma_{1,2}$  we take into account the expected identification efficiencies,  $\epsilon$  [13] and the systematic uncertainties,  $\delta^{\text{sys}}$ , on the various fermionic final states, for which we assume: for leptons:  $\epsilon = 95\%$  and  $\delta^{\text{sys}} = 0.5\%$ ; for  $b$  quarks:  $\epsilon = 60\%$  and  $\delta^{\text{sys}} = 1\%$ ; for  $c$  quarks:  $\epsilon = 35\%$  and  $\delta^{\text{sys}} = 1.5\%$ . As concerns the systematic uncertainty, we assume the same  $\delta^{\text{sys}}$  for  $i = 1, 2$ , and independent of  $z^*$  in the relevant angular range.

We consider the LC with the following options:  $\sqrt{s} = 0.5$  TeV,  $\mathcal{L}_{\text{int}} = 50 \text{ fb}^{-1}$ ,  $P = 0.8$  and  $|\cos\theta| \leq 0.99$ . We assume half the total integrated luminosity quoted above for both values of the electron polarization,  $P_e = \pm P$ . As an example, the relative uncertainties,  $\delta\sigma_{\alpha\beta}/\sigma_{\alpha\beta}$ , on the helicity cross sections for the process  $e^+e^- \rightarrow \mu^+\mu^-$ , are shown as functions of  $z^*$  in Fig. 1. The optimal kinematical parameters  $z_{\text{opt}}^*$  where the sensitivity of leptonic process is a maximum, can easily be obtained from this figure. The corresponding dependences for quark final states are analogous.

In order to assess the increase of sensitivity obtained by optimization, one should compare the corresponding uncertainties at  $z_{\text{opt}}^*$  with those obtained without optimization, at  $z_{\pm}^*$  of Eq. (11). Fig. 1, show that, in the LL and RR cases, optimization results in a rather modest increase of sensitivity and

of the corresponding discovery limits on  $\Lambda_{\text{RR}}$  and  $\Lambda_{\text{LL}}$  (by a few percent), since the  $z^*$  behavior of the uncertainty is rather flat. Conversely, in the LR and RL cases optimization can substantially increase the sensitivity and the corresponding reachable lower bounds on  $\Lambda_{\text{LR}}$  and  $\Lambda_{\text{RL}}$  (up to a factor of about 2 for the  $c\bar{c}$  case).

The bounds on the contact interaction parameters can be obtained by using  $\chi^2$  procedure. In the numerical analysis presented below, we take three different values of the polarization,  $P = 1, 0.8, 0.5$ , in order to study this dependence. This is a reasonable variation around the value  $P = 0.8$  expected at the LC [14]. Table 1 shows that the helicity cross sections  $\sigma_{\alpha\beta}$  are quite sensitive to contact interactions,

Table 1: Contact-interaction reach (in TeV) at an  $e^+e^-$  linear collider with  $E_{\text{c.m.}} = 0.5$  TeV and  $\mathcal{L}_{\text{int}} = 50 \text{ fb}^{-1}$ , at 95% C.L. Radiative corrections are included, with a cut on the energy of photons emitted in the initial state. The arrows indicate the increase of sensitivity of the observables caused by the optimization.

process	$P$	$\Lambda_{\text{LL}}$	$\Lambda_{\text{RR}}$	$\Lambda_{\text{LR}}$	$\Lambda_{\text{RL}}$
$\mu^+\mu^-$	1.0	$40 \rightarrow 41$	$39 \rightarrow 40$	$26 \rightarrow 40$	$28 \rightarrow 41$
	0.8	$37 \rightarrow 38$	$37 \rightarrow 38$	$25 \rightarrow 37$	$26 \rightarrow 37$
	0.5	$32 \rightarrow 32$	$31 \rightarrow 32$	$21 \rightarrow 30$	$21 \rightarrow 30$
$\bar{b}b$	1.0	$41 \rightarrow 42$	$45 \rightarrow 47$	$17 \rightarrow 31$	$34 \rightarrow 42$
	0.8	$40 \rightarrow 41$	$38 \rightarrow 39$	$17 \rightarrow 29$	$29 \rightarrow 38$
	0.5	$36 \rightarrow 37$	$29 \rightarrow 29$	$13 \rightarrow 25$	$22 \rightarrow 31$
$\bar{c}c$	1.0	$32 \rightarrow 33$	$36 \rightarrow 37$	$21 \rightarrow 32$	$20 \rightarrow 30$
	0.8	$31 \rightarrow 32$	$32 \rightarrow 33$	$20 \rightarrow 31$	$18 \rightarrow 27$
	0.5	$27 \rightarrow 28$	$26 \rightarrow 27$	$18 \rightarrow 27$	$15 \rightarrow 22$

with discovery limits ranging from 40 to 80 times the CM energy at the degree of electron polarization  $P = 0.8$ . The best sensitivity occurs for the  $\bar{b}b$  final state, while the worst one is for  $\bar{c}c$ . Decreasing the electron polarization from  $P = 1$  to  $P = 0.5$  results in a worsening of the sensitivity by 20 – 40%, depending on the final state. Regarding the role of the assumed uncertainties on the observables under consideration, in the cases of  $\Lambda_{\text{LR}}$  and  $\Lambda_{\text{RL}}$  the expected statistics are such that the uncertainty turns out to be dominated by the statistical one, and the results have little sensitivity to the value of the systematic uncertainty. Conversely, in the cases of  $\Lambda_{\text{LL}}$  and  $\Lambda_{\text{RR}}$  the results depend more sensitively on the assumed value of the systematic uncertainty. Moreover, as is evident from Eqs. (5) and (6), a further improvement in the sensitivity to the various  $\Lambda$ -scales in Table 1 would be obtained if both  $e^-$  and  $e^+$  longitudinal polarizations were available.

### 3 Constraints and resolving power on $Z'$

As mentioned in the Introduction, also the  $s$ -channel exchange of a new, very massive, neutral gauge boson  $Z'$  with  $\sqrt{s} \ll M_{Z'}$  can be identified to a contact interaction Lagrangian of the kind in Eq. (2). Specifically, the contribution of the  $Z'$ -mediated helicity amplitudes, to be added to the SM ones, takes the form:

$$A_{\alpha\beta}(Z') = g'^e_\alpha g'^f_\beta \chi_{Z'} \simeq -g'^e_\alpha g'^f_\beta \frac{s}{M_{Z'}^2} \left( 1 + \frac{s}{M_{Z'}^2} + \dots \right), \quad (27)$$

where  $\chi_{Z'} = s/(s - M_{Z'}^2)$  is the  $Z'$  propagator, and  $g'^e_\alpha$ ,  $g'^f_\alpha$  are the fermionic couplings of the  $Z'$  [8, 9]:

$$g'^f_L = \frac{g_{Z'}}{e} L_{Z'}^f, \quad g'^f_R = \frac{g_{Z'}}{e} R_{Z'}^f. \quad (28)$$

Comparing Eqs. (7) and (27), one finds

$$\frac{\eta_{\alpha\beta}}{\Lambda_{\alpha\beta}^2} \approx -g'^e_\alpha g'^f_\beta \frac{\alpha}{M_{Z'}^2}. \quad (29)$$

Thus, in the case of no observed signal, i.e., no deviation of  $\sigma_{\alpha\beta}$  from the SM prediction within the experimental accuracy, at given  $M_{Z'}$  one can directly obtain model-independent bounds on the fermionic chiral couplings to the  $Z'$  from Eqs.(27)-(29) and the constraints listed in Table 1.

If a  $Z'$  is indeed discovered, perhaps at a hadron machine, it becomes interesting to measure as accurately as possible its couplings and mass at the LC, and make tests of the various extended gauge models. Another interesting question is the potential of the leptonic process (1) to identify the  $Z'$  model underlying the measured signal, through the measurement of the helicity cross sections, e.g.  $\sigma_{RR}$  and  $\sigma_{LL}$ . Such cross sections only depend on the relevant leptonic chiral coupling and on  $M_{Z'}$ , so that such resolving power clearly depends on the actual value of the  $Z'$  mass. In Figs. 2a and 2b we show this dependence for the  $E_6$  and the  $LR$  models of interest here. In these figures, the horizontal lines represent the values of the couplings predicted by the various models, and the lines joining the upper and the lower ends of the vertical bars represent the expected experimental uncertainty at the 95% CL. The intersection of the lower such lines with the  $M_{Z'}$  axis determines the discovery reach for the corresponding model: larger values of  $M_{Z'}$  would determine a  $Z'$  signal smaller than the experimental uncertainty and, consequently, statistically invisible. Also, Figs. 2a and 2b show the complementary roles of  $\sigma_{LL}$  and  $\sigma_{RR}$  to set discovery limits: while  $\sigma_{LL}$  is mostly sensitive to the  $Z'_\chi$  and has the smallest sensitivity to the  $Z'_\eta$ ,  $\sigma_{RR}$  provides the best limit for the  $Z'_{LR}$  and the worst one for the  $Z'_\chi$ .

As Figs. 2a and 2b show, the different models can be distinguished by means of  $\sigma_{\pm}$  as long as the uncertainty of the coupling of one model does not overlap with the value predicted by the other model. Thus, the identification power of the leptonic process (1) is determined by the minimum  $M_{Z'}$  value at which such ‘confusion region’ starts. For example, Fig. 2a shows that the  $\chi$  model cannot be distinguished from the  $LR$ ,  $\psi$  and  $\eta$  models at  $Z'$  masses larger than 2165 GeV, 2270 GeV and 2420 GeV, respectively. The identification power for the typical models are indicated in Figs. 2a and 2b by the symbols circle, diamond, square and triangle.

In the case of process (1) with  $\bar{q}q$  pair production (with  $q = c, b$ ), the analysis is complicated by the fact that the relevant helicity amplitudes depend on three parameters ( $g_\alpha^{qe}$ ,  $g_\beta^{q\bar{q}}$  and  $M_{Z'}$ ) instead of two. Nevertheless, there is still some possibility to derive general information on the  $Z'$  chiral couplings to quarks. As an illustrative example, in Fig. 3 we depict the bounds from the process  $e^+e^- \rightarrow b\bar{b}$  in the  $(L_{Z'}^e, L_{Z'}^b)$  and  $(L_{Z'}^e, R_{Z'}^b)$  planes for the  $Z'$  of the  $\chi$  model, with  $M_{Z'} = 1$  TeV. Taking into account two-fold ambiguity, the allowed regions are the ones included within the two sets of hyperbolic contours in the upper-left and in the lower-right corners of Fig. 3. Then, to get finite regions for the quark couplings, one must combine the hyperbolic regions so obtained with the determinations of the leptonic  $Z'$  couplings from the leptonic process (1), represented by the two vertical strips. The corresponding shaded areas represent the determinations of  $L_{Z'}^b$ , while the hatched areas are the determinations of  $R_{Z'}^b$ . Notice that, in general, there is the alternative possibility of deriving constraints on quark couplings also in the case of right-handed electrons, namely, from the determinations of the pairs of couplings  $(R_{Z'}^e, L_{Z'}^b)$  and  $(R_{Z'}^e, R_{Z'}^b)$ . However, as observed with regard to the previous analysis of the leptonic process, the sensitivity to the right-handed electron coupling turns out to be smaller than for  $L_{Z'}^e$ , so that the corresponding constraints are weaker.

## 4 Summary

We emphasize that the measurement of the helicity cross sections of the process (1) with optimal kinematical cuts could substantially increase their sensitivity to contact interaction parameters and could give crucial, model-independent information on the chiral structure of such new interactions.

As an application of the proposed approach at LC, we study the sensitivity to  $Z'$ . In the case of no observed signal, one can directly obtain model-independent bounds on the leptonic chiral couplings of the  $Z'$  from  $e^+e^- \rightarrow l^+l^-$  and on the products of lepton-quark chiral couplings from  $e^+e^- \rightarrow \bar{q}q$  (with  $l = \mu, \tau$  and  $q = c, b$ ). In the case  $Z'$  manifestations are observed as deviations from the SM, the role of  $\sigma_{\alpha\beta}$  is more interesting, specially as regards the problem of identifying the various models as potential sources of such non-standard effects. Indeed, in principle, they provide a unique possibility to disentangle and extract numerical values for the chiral couplings of the  $Z'$  in a general way, avoiding the danger of cancellations, so that  $Z'$  model predictions can be tested.

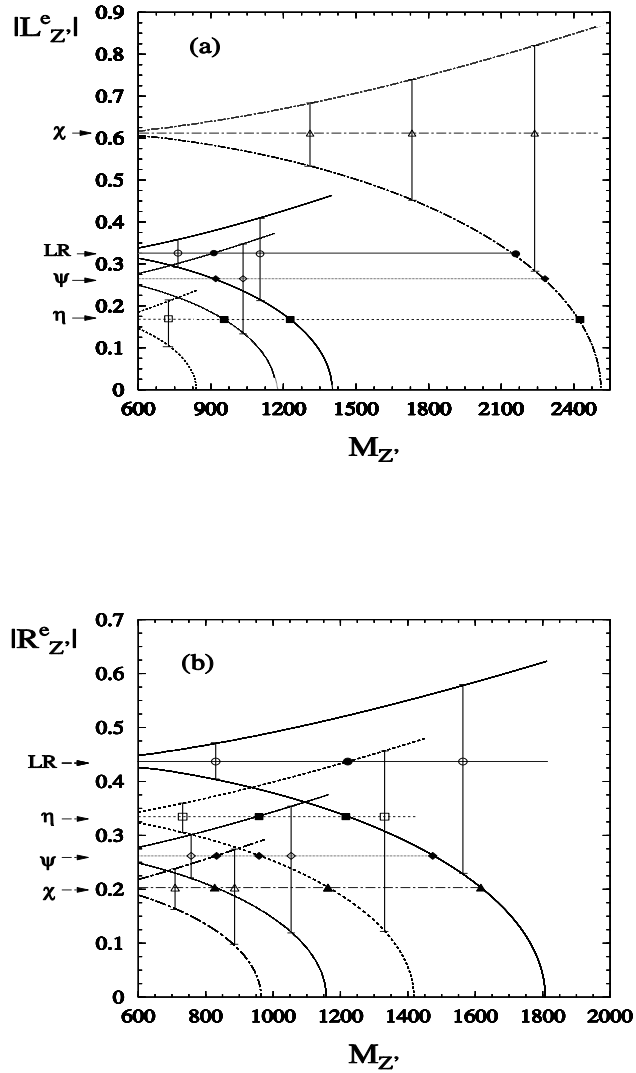


Figure 2: Resolution power at 95% C.L. for the absolute value of the leptonic  $Z'$  couplings,  $|L_{Z'}^e|$  (a) and  $|R_{Z'}^e|$  (b), as a function of  $M_{Z'}$ , obtained from  $\sigma_{LL}$  and  $\sigma_{RR}$ , respectively, in process  $e^+e^- \rightarrow l^+l^-$ . The error bars combine statistical and systematic uncertainties. Horizontal lines correspond to the values predicted by typical models.

## Acknowledgements

I would like to thank P. Osland, N. Paver and A.A. Babich for the fruitful and enjoyable collaboration on the subject matter covered here.

## References

- [1] E.J. Eichten, K.D. Lane and M.E. Peskin, Phys. Rev. Lett. **50** (1983) 811.
- [2] R.J. Cashmore, et al., Phys. Rept. **122** (1985) 275; R. Rückl, Phys. Lett. **B129** (1983) 363.

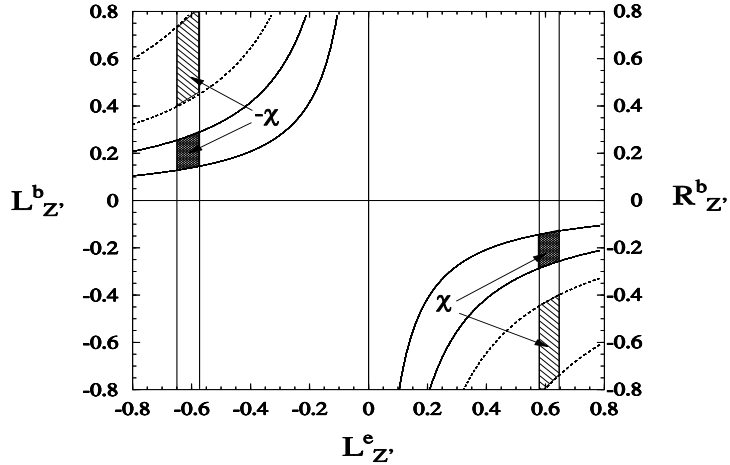


Figure 3: Allowed bounds at 95% C.L. on  $Z'$  couplings with  $M_{Z'} = 1$  TeV ( $\chi$  model) in the two-dimension planes  $(L_{Z'}^e, L_{Z'}^b)$  and  $(L_{Z'}^e, R_{Z'}^b)$  obtained from helicity cross sections  $\sigma_{LL}$  (solid lines) and  $\sigma_{LR}$  (dashed lines), respectively. The shaded and hatched regions are derived from the combination of  $e^+e^- \rightarrow l^+l^-$  and  $e^+e^- \rightarrow \bar{b}b$  processes.

- [3] P. Haberl, F. Schrempp, and H.-U. Martyn, in *Physics at HERA*, Proceedings of the workshop, Vol. 2 (1991) p.1133;
- [4] G. Altarelli, J. Ellis, G.F. Giudice, S. Lola, and M.L. Mangano, Nucl. Phys. **B506** (1997) 3;
- [5] V. Barger, K. Cheung, K. Hagiwara, and D. Zeppenfeld, Phys. Lett. **B404** (1997) 147;
- [6] J. Kalinowski, R. Rückl, H. Spiesberger, and P.M. Zerwas, Phys. Lett. **B406** (1997) 314; Z. Phys. **C 74** (1997) 595.
- [7] V. Barger, K. Cheung, K. Hagiwara, and D. Zeppenfeld, Phys. Rev. D **57** (1998) 391; D. Zeppenfeld and K. Cheung, preprint MADPH-98-1081, hep-ph/9810277.
- [8] P. Osland and A.A. Pankov, Phys. Lett. **B 403** (1997) 93; **B 406** (1997) 328.
- [9] A.A. Babich, A.A. Pankov, and N. Paver, Phys. Lett. **B 426** (1998) 375; **B 452** (1999) 355.
- [10] A.A. Pankov and N. Paver, Phys. Lett. **B 432** (1998) 159.
- [11] S. Riemann, FORTRAN program ZEFIT Version 4.2; D. Bardin et al., preprint CERN-TH. 6443/92, CERN (1992).
- [12] A. Djouadi, A. Leike, T. Riemann, D. Schaile and C. Verzegnassi, Z. Phys. **C56** (1992) 289.
- [13] C.J.S. Damerell and D.J. Jackson, in *Proceedings of the 1996 DPF/DPB Summer Study on New Directions for High Energy Physics* (Snowmass 96), Edited by D.G. Cassel, L. Trindle Gennari, R.H. Siemann (SLAC, 1997) p. 442.
- [14] E. Accomando et al. (ECFA/DESY LC Physics Working Group), Phys. Rept. **299** (1998) 1.